THE JOURNAL OF BIOLOGICAL CHEMISTRY VOL. 286, NO. 5, pp. 3351–3358, February 4, 2011

Structural Determinants of Affinity Enhancement between GoLoco Motifs and G-Protein α Subunit Mutants*[S]

Received for publication, October 1, 2010, and in revised form, November 1, 2010 Published, JBC Papers in Press, November 29, 2010, DOI 10.1074/jbc.M110.190496

Dustin E. Bosch[‡1], Adam J. Kimple[‡1], Deanne W. Sammond[§], Robin E. Muller[‡], Michael J. Miley[‡], Mischa Machius[‡], Brian Kuhlman[§], Francis S. Willard[‡2], and David P. Siderovski[‡¶‖3]

From the Departments of [‡]Pharmacology and [§]Biochemistry and Biophysics, [¶]University of North Carolina Neuroscience Center, and [‖]Lineberger Comprehensive Cancer Center, University of North Carolina, Chapel Hill, North Carolina 27599

GoLoco motif proteins bind to the inhibitory G_i subclass of G-protein α subunits and slow the release of bound GDP; this interaction is considered critical to asymmetric cell division and neuro-epithelium and epithelial progenitor differentiation. To provide protein tools for interrogating the precise cellular role(s) of GoLoco motif/$G\alpha_i$ complexes, we have employed structure-based protein design strategies to predict gain-of-function mutations that increase GoLoco motif binding affinity. Here, we describe fluorescence polarization and isothermal titration calorimetry measurements showing three predicted $G\alpha_{i1}$ point mutations, E116L, Q147L, and E245L; each increases affinity for multiple GoLoco motifs. A component of this affinity enhancement results from a decreased rate of dissociation between the Gα mutants and GoLoco motifs. For $G\alpha_{i1}^{Q147L}$, affinity enhancement was seen to be driven by favorable changes in binding enthalpy, despite reduced contributions from binding entropy. The crystal structure of $G\alpha_{i1}^{Q147L}$ bound to the RGS14 GoLoco motif revealed disorder among three peptide residues surrounding a well defined Leu-147 side chain. Monte Carlo simulations of the peptide in this region showed a sampling of multiple backbone conformations in contrast to the wild-type complex. We conclude that mutation of Glu-147 to leucine creates a hydrophobic surface favorably buried upon GoLoco peptide binding, yet the hydrophobic Leu-147 also promotes flexibility among residues 511–513 of the RGS14 GoLoco peptide.

Protein-based therapeutics and tools are increasingly utilized for manipulating cell biology (1–5). A vital aspect of their effective function is affinity for a target protein or ligand. An effective approach for enhancing the affinity of protein/protein interactions is structure-based computational prediction of affinity-enhancing point mutations (6–9). The development of reliable *in silico* procedures promises to provide a more efficient means of protein design than labor-intensive combinatorial screening techniques such as phage display or ribosome display (10–12). Previously, a structure-based protocol for predicting affinity-enhancing point mutations was developed (7), in part using as a template the high-resolution crystal structure of the heterotrimeric G-protein subunit $G\alpha_{i1}$ in complex with the RGS14 (regulator of G-protein signaling 14) GoLoco motif (13). Residues at the protein/peptide binding surface were sequentially mutated to nonpolar amino acids *in silico*, producing 33 predicted affinity-enhancing mutations. Four of six experimentally tested mutations to either $G\alpha_{i1}$ or the GoLoco motif enhanced binding affinity, as predicted by Rosetta (7).

As a critical component of seven-transmembrane domain receptor signaling, Gα subunits normally cycle between an inactive GDP-bound state and an active GTP-bound state (reviewed in Refs. 14 and 15). GoLoco motif proteins such as LGN, AGS3, RGS12, and RGS14 act as guanine nucleotide dissociation inhibitors, specifically for the adenylyl cyclase inhibitory subclass of Gα subunits (reviewed in Refs. 16 and 17). GoLoco motifs prevent GDP dissociation by binding across the Ras-like and all-helical domains of Gα, as well as by contributing an arginine side chain from the highly conserved (E/D)QR GoLoco triad (16) to contacts made to the bound guanosine diphosphate (13). Not only are GoLoco motif-containing proteins thought to modulate seven-transmembrane domain receptor signaling in various physiological responses (18–20), but these proteins are also critical to cell fate determinant sorting and cell division processes in multiple contexts across multiple species (21–24). Highlighting the value of mutation-derived affinity modulation to cell biological applications, a $G\alpha_{i1}^{N149I}$ mutant with selective loss of GoLoco motif affinity has recently provided direct evidence for the $G\alpha_i$/GoLoco protein interaction in these cell division processes (25, 26).

We previously predicted that mutation to leucine of one of three polar residues, Glu-116, Gln-147, or Glu-245, on the surface of $G\alpha_{i1}$ enhances binding of $G\alpha_{i1}$-GDP to the RGS14 GoLoco motif (7, 27). Although the algorithms implemented in the Rosetta program predict a favorable change in the Gibbs free energy of binding, our computational tools do not provide a clear mechanism of affinity enhancement. Knowledge of changes in the thermodynamic and/or kinetic parameters of binding, such as the rate of dissociation, will be im-

* This work was supported, in whole or in part, by National Institutes of Health Grants R01 CA127152 (to D. P. S.), F30 MH074266 (to A. J. K.), and T32 GM008719 (to D. E. B. and A. J. K.).

[S] The on-line version of this article (available at http://www.jbc.org) contains supplemental Figs. S1–S3 and Table S1.

The atomic coordinates and structure factors (code 3ONW) have been deposited in the Protein Data Bank, Research Collaboratory for Structural Bioinformatics, Rutgers University, New Brunswick, NJ (http://www.rcsb.org/).

[1] Both authors contributed equally to this work.

[2] To whom correspondence may be addressed: Lilly Research Laboratories, Eli Lilly and Co., Indianapolis, IN 46285. E-mail: francis.willard@gmail.com.

[3] To whom correspondence may be addressed: University of North Carolina, 4073 Genetic Medicine Bldg., 120 Mason Farm Rd., CB#7365, Chapel Hill, NC 27599. Tel.: 919-843-9363; Fax: 919-966-5640; E-mail: dsiderov@med.unc.edu.

portant in the future application of these computational design strategies to biological and therapeutic questions. Here, we assessed the effects of these predicted $G\alpha_{i1}$/GoLoco affinity-enhancing mutations on the kinetics and thermodynamics of binding using fluorescence polarization, isothermal titration calorimetry, and surface plasmon resonance. Although mutations that promote binding to a target protein are desirable, protein design applications often require the preservation of other protein functions. Accordingly, we also determined the effects of these three affinity-enhancing mutations on the nucleotide cycle of $G\alpha_{i1}$, including GTP binding and hydrolysis. To further elucidate the molecular mechanism of affinity enhancement for one mutant, we determined the x-ray crystal structure of $G\alpha_{i1}{}^{Q147L}$-GDP bound to the RGS14 GoLoco motif. In addition, we investigated the conformational flexibility of the GoLoco peptide backbone and side chains surrounding the Leu-147 residue of the $G\alpha_{i1}$ mutant using Monte Carlo simulations.

EXPERIMENTAL PROCEDURES

Chemicals and Other Assay Materials—Unless otherwise noted, all chemicals were the highest grade available from Sigma or Fisher Scientific. Peptides were synthesized by Fmoc (*N*-(9-fluorenyl)methoxycarbonyl) group protection, purified via HPLC, and confirmed using mass spectrometry by the Tufts University Core Facility (Medford, MA). Peptide sequences are as follows: FITC-GPSM2(GL2), FITC-β-alanine-NTDEFLDLLASSQSRRLDDQRASFSNLPGLRLTQNSQS-amide; FITC-RGS12 GoLoco, FITC-β-alanine-DEAEEFFELI-SKAQSNRADDQRGLLRKEDLVLPEFLR-amide; FITC-RGS14 GoLoco, FITC-β-alanine-SDIEGLVELLNRVQSSGA-HDQRGLLRKEDLVLPEFLQ-amide; and RGS14 GoLoco, DIEGLVELLNRVQSSGAHDQRGLLRKEDLVLPEFLQ-amide.

Protein Expression and Purification—For biochemical experiments, N-terminally truncated, hexahistidine-tagged WT and mutant $G\alpha_{i1}$ proteins were expressed and purified as described previously (28). Point mutations were made using QuikChange site-directed mutagenesis (Stratagene, La Jolla, CA). For crystallization, the $G\alpha_{i1}{}^{Q147L}$ mutant was expressed and purified as described previously (29). Purified $G\alpha_{i1}{}^{Q147L}$ was concentrated to 15 mg/ml and stored in crystallization buffer (10 mM Tris (pH 7.5), 1 mM magnesium chloride, 5% (v/v) glycerol, and 5 mM DTT).

Fluorescence Polarization Measurements—All polarization experiments were conducted using a PHERAstar microplate reader (BMG Labtech, Offenburg, Germany). Excitation wavelength was 485 ± 6 nm, and emission was recorded at 520 ± 15 nm. Gains of the parallel and perpendicular channels were calibrated so that 350 pM FITC probe alone had a polarization of ~35 milli-Polarization units (mP) for each experiment. All experiments were conducted at 25 °C in triplicate using 96-well black-bottom plates (Costar, Corning, NY). The final volume of each well was brought to 180 μl with PheraBuffer (10 mM Tris (pH 7.5), 150 mM NaCl, 100 μM GDP, and 0.05% (v/v) Nonidet P-40). For experiments conducted in the presence of the transition-state mimetic, aluminum magnesium tetrafluoride (AMF),[4] an additional 10 mM $MgCl_2$, 10 mM NaF, and 30 μM $AlCl_3$ were added to the standard PheraBuffer. Polarization was determined from raw intensity values of the parallel and perpendicular channels using PHERAstar Version 1.60 software (BMG Labtech). Binding isotherms were fit and equilibrium dissociation constants were determined using GraphPad Prism Version 5.0 as described previously (28).

Surface Plasmon Resonance Assays—Optical detection of protein/protein interactions by surface plasmon resonance was performed using a Biacore 3000 (GE Healthcare). Carboxymethylated dextran (CM5) sensor chips (GE Healthcare) with covalently bound anti-GST antibody surfaces were created as described previously (30). The GST-GoLoco fusion proteins GST-RGS12 (amino acids 1184–1228) (29), GST-RGS14 (amino acids 497–532) (29), and GST-GPSM2(GL2) (31), as well as GST alone (serving as a negative control), were loaded onto separate surfaces to levels of 1372, 963, 1290, and 1061 resonance units (RU), respectively. All experiments were performed with the sensor surface, fluidics, and pump equilibrated with Biacore running buffer (10 mM HEPES (pH 7.4), 150 mM NaCl, 0.05% (v/v) Nonidet P-40, 100 μM GDP, and 50 μM EDTA). Injections of 200 μl of WT or mutant $G\alpha_{i1}$ at 50 μM for kinetic analyses were performed using the KINJECT command with a dissociation phase of 2000 s at a flow rate of 40 μl/min. The surface was regenerated between runs by removal of bound $G\alpha_{i1}$ using 325-μl injections of AMF buffer (Biacore running buffer with an additional 10 mM $MgCl_2$, 10 mM NaF, and 30 μM $AlCl_3$). Nonspecific binding to the GST only-loaded surface was subtracted from each curve (BIAevaluation Version 3.0 software, GE Healthcare). To establish off-rates, dissociation-phase sensorgrams were normalized to percent bound, and the averages of triplicate experiments were fit to a single exponential function for dissociation without constraints using Prism Version 5.0.

Nucleotide Binding and Hydrolysis Assays—The [^{35}S]GTPγS filter-binding assay used to measure rates of spontaneous GDP release was conducted as described previously (32). Briefly, WT or mutant $G\alpha_{i1}$ (100 nM) was incubated in assay buffer (20 mM Tris (pH 7.5), 1 mM $C_{12}E_{10}$, 1 mM DTT, 1 mM EDTA, 100 mM NaCl, and 25 mM $MgCl_2$) or nonspecific buffer (assay buffer plus 100 μM GTPγS) at 20 °C. Radioligand binding was initiated by the addition of 6.25 nM [^{35}S]GTPγS. At timed intervals, 100-μl aliquots of the reaction were filtered through nitrocellulose membranes and washed four times with 7.5 ml of ice-cold wash buffer (20 mM Tris (pH 7.5), 120 mM NaCl, and 25 mM $MgCl_2$). Filters were dried under a vacuum before measuring β-radiation via liquid scintillation counting.

Intrinsic GTP hydrolysis rates of $G\alpha_{i1}$ subunits were assessed by monitoring the production of ^{32}P-labeled inorganic phosphate during a single round of GTP hydrolysis as described previously (33). In brief, WT or mutant $G\alpha_{i1}$ (100 nM) was incubated for 10 min at 20 °C with 1×10^6 cpm of

[4] The abbreviations used are: AMF, aluminum magnesium tetrafluoride; GTPγS, guanosine 5′-*O*-(thiotriphosphate); ITC, isothermal titration calorimetry; FP, fluorescence polarization; CI, confidence interval.

[γ-^{32}P]GTP (specific activity of 6500 dpm/Ci; PerkinElmer Life Sciences) in reaction buffer (50 mM Tris (pH 7.5), 0.05% (v/v) $C_{12}E_{10}$, 1 mM DTT, 10 mM EDTA, 100 mM NaCl, and 5 μg/ml BSA). The nucleotide-loaded protein was then chilled on ice for 5 min prior to initiation of hydrolysis by the addition of 10 mM $MgCl_2$ and 100 μM GTPγS (final concentrations). At timed intervals, 100-μl aliquots were quenched in 900 μl of charcoal slurry (5% (w/v) activated charcoal in 50 mM H_3PO_4 (pH 3.0)) and centrifuged at 4 °C for 10 min at 4000 × *g*. Subsequently, the β-radiation of 600-μl aliquots of the supernatant was counted via liquid scintillation.

Intrinsic Tryptophan Fluorescence Measurements of Gα Activation—Changes in tryptophan fluorescence of $G\alpha_{i1}$ subunits were measured to assess activation by the transition-state mimetic GDP·AlF_4^-. Activation of $G\alpha_{i1}$ results in translocation of Trp-211, a residue in the conformationally flexible switch II region, to a hydrophobic pocket; the change in environment results in an increased quantum yield of Trp-211 fluorescence (34, 35). Tryptophan fluorescence of WT or mutant $G\alpha_{i1}$ (1 μM) was measured using a POLARstar Omega plate reader (BMG Labtech) in 187 μl of assay buffer (100 mM NaCl, 100 μM EDTA, 2 mM $MgCl_2$, 2 μM GDP, and 20 mM Tris (pH 8.0)). Intrinsic fluorescence was measured using a 280-nm excitation filter and 350-nm emission filter (each with 10-nm cutoffs). After a 20-s equilibration at ambient temperature, activation was induced by sequential injections of 8 μl of 0.5 M NaF and 5 μl of 1.2 mM $AlCl_3$ to each well. Tryptophan fluorescence was recorded for 2 min following activation. Fluorescence intensity traces shown represent the average of experiments performed in triplicate.

Isothermal Titration Calorimetry—Isothermal titration calorimetry (ITC) was performed using a MicroCal™ Auto-ITC200 system (GE Healthcare). WT and mutant $G\alpha_{i1}$ subunits were subjected to size-exclusion chromatography in ITC buffer (50 mM HEPES (pH 7.5), 150 mM NaCl, 10 μM GDP, 5% (v/v) glycerol, and 0.005% (v/v) β-mercaptoethanol) and subsequently concentrated to 30 μM using a VivaSpin 20 ultrafiltration spin column (Sartorius Stedim Biotech, Göttingen, Germany) at 4 °C and 3000 × *g*. Lyophilized RGS14 GoLoco peptide was dissolved in ITC buffer to a concentration of 350 μM. Titrations were performed at 25 °C and consisted of 20 2-μl injections of peptide into WT $G\alpha_{i1}$ or $G\alpha_{i1}^{Q147L}$ solutions at 250-s intervals. Binding isotherms and curve fittings were obtained using Origin for ITC analysis software (MicroCal). Enthalpy of binding was determined for three titrations each of RGS14 GoLoco peptide into solutions of wild-type $G\alpha_{i1}$ or $G\alpha_{i1}^{Q147L}$, and average values were compared with a Student's *t* test using Prism Version 5.0. Because ITC sensitivity did not allow us to approach a $G\alpha_{i1}$ or peptide concentration near the K_D, Gibbs free energy of binding was calculated from the more accurate fluorescence polarization binding affinity measurements, using $\Delta G = -R(T)\ln(1/K_D)$, where R is the universal gas constant and T is temperature in Kelvin. Entropy of binding was then estimated with $\Delta S = (\Delta H - \Delta G)/T$, where ΔH is the average enthalpy of binding derived from isothermal titrations.

Crystallization and Structure Determination—The complex of $G\alpha_{i1}^{Q147L}$ and RGS14 GoLoco peptide was obtained by mixing $G\alpha_{i1}^{Q147L}$ and GoLoco peptide to concentrations of 400 and 600 μM, respectively, in 10 mM Tris (pH 7.5), 1 mM $MgCl_2$, 10 μM GDP, 5% (v/v) glycerol, and 5 mM DTT. Crystals of the $G\alpha_{i1}^{Q147L}$·GDP/GoLoco peptide heterodimer were obtained by vapor diffusion from hanging drops containing a 1:1 (v/v) ratio of protein/peptide solution to well solution (1.5–1.6 M ammonium sulfate, 100 mM $MgCl_2$, 100 mM sodium acetate (pH 4.8), and 10% (v/v) glycerol). Crystals (~200 × 200 × 50 μm) formed in 1–4 days at 18 °C exhibited the symmetry of space group $P222_1$ (a = 70.3, b = 83.7, and c = 190.1 Å, $\alpha = \beta = \gamma = 90°$) and contained two $G\alpha_{i1}^{Q147L}$/GoLoco heterodimers in the asymmetric unit. For data collection at 100 K, crystals were transferred to well solution supplemented with 25% saturated sucrose for ~30 s, followed by plunging into liquid nitrogen. A native data set was collected at the SER-CAT 22-BM beamline at the Advanced Photon Source (Argonne National Laboratory). Data were processed using the HKL-2000 program (36). The crystal structure of the WT $G\alpha_{i1}$/RGS14 GoLoco heterodimer (Protein Data Bank code 2OM2 (7)), excluding the GoLoco motif peptide, nucleotide, waters, and magnesium, was used as a search model for molecular replacement using the Phaser program (37). Refinement was carried out using the Refmac5 program (38), consisting of conjugate gradient minimization and refinement of individual atomic displacement and translation-libration-screw parameters, interspersed with manual revisions of the model using the Coot program (39). The current model contains two $G\alpha_{i1}^{Q147L}$·GDP/GoLoco peptide heterodimers in the asymmetric unit. For data collection and refinement statistics and a list of residues that could not be located in the electron density, see supplemental Table S1. All structural images were made with PyMOL (Schrödinger LLC, Portland, OR) unless indicated otherwise.

RESULTS AND DISCUSSION

Comparing Different Point Mutations in $G\alpha_{i1}$ That Enhance Affinity for GoLoco Motifs—Three polar-to-nonpolar point mutations in $G\alpha_{i1}$ (E116L, Q147L, and E245L) have been described individually (7, 27) as enhancing GoLoco motif binding affinity; the location of these three positions within $G\alpha_{i1}$ is highlighted in supplemental Figs. S1 and S2. To determine and compare directly the affinities of these three separate $G\alpha_{i1}$ point mutants ($G\alpha_{i1}^{E116L}$, $G\alpha_{i1}^{Q147L}$, and $G\alpha_{i1}^{E245L}$) for the GoLoco motif of RGS14, we used a synthetic FITC-RGS14 GoLoco motif peptide probe in fluorescence polarization (FP) binding assays similar to those performed with RGS12 and WT $G\alpha_{i1}$ (28). Holding the peptide concentration at 350 pM, we added increasing concentrations of WT or mutant $G\alpha_{i1}$ protein (30 pM to 200 nM) and generated equilibrium binding isotherms (Fig. 1). The dissociation constants (K_D) were determined to be 14, 1.6, 2.3, and 0.69 nM for GDP-bound $G\alpha_{i1}^{WT}$, $G\alpha_{i1}^{E116L}$, $G\alpha_{i1}^{Q147L}$, and $G\alpha_{i1}^{E245L}$, respectively. These results confirm our earlier reports of affinity enhancement obtained with a tenascin-GoLoco fusion FP probe (7) and, for $G\alpha_{i1}^{E245L}$, mutation in the context of other affinity-modifying changes (27). Consistent with the selective binding of GoLoco motifs to ground-state $G\alpha_i$ subunits (*i.e.* $G\alpha_i$·GDP) (reviewed in Ref. 16), the transition-state mimetic form (*i.e.*

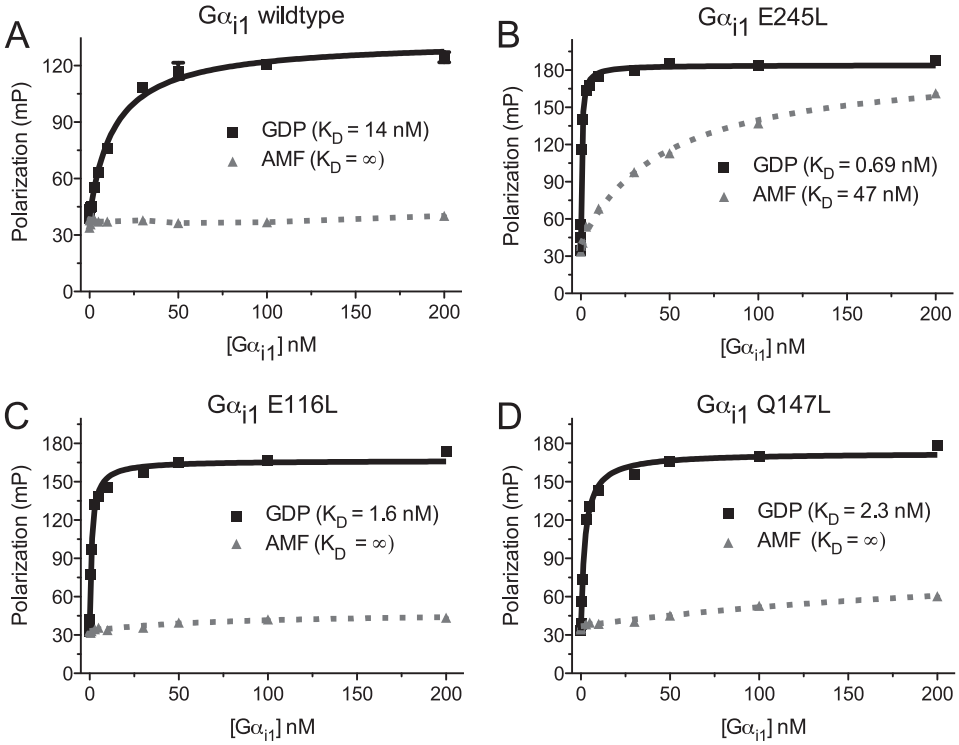

FIGURE 1. **WT Gα$_{i1}$ and three affinity-enhanced mutants bind to the RGS14 GoLoco motif in a nucleotide-dependent manner.** Binding isotherms were generated using FP measurements by increasing the concentration of Gα$_{i1}$ protein while maintaining the concentration of FITC-labeled RGS14 GoLoco motif peptide constant at 350 pM. All experiments were performed in triplicate. The *error bars* represent S.E. *A*, Gα$_{i1}$^{WT}·GDP binds the RGS14 GoLoco motif with a dissociation constant (K_D) of 14 nM (95% CI, 11–17 nM). No appreciable binding was observed when the Gα$_{i1}$ protein was in its transition-state mimetic form, created with AMF. *B*, Gα$_{i1}$^{E245L} binds the RGS14 GoLoco motif with K_D values of 0.69 nM (95% CI, 0.61–0.77 nM) and 47 nM (95% CI, 37–56 nM) in its GDP and GDP·AMF forms, respectively. *C*, Gα$_{i1}$^{E116L}·GDP binds the RGS14 GoLoco motif with a K_D of 1.6 nM (95% CI, 1.4–1.7 nM), whereas no appreciable binding is observed with the AMF-activated Gα$_{i1}$^{E116L}. *D*, Gα$_{i1}$^{Q147L}·GDP binds the RGS14 GoLoco motif with a K_D of 2.3 nM (95% CI, 1.9–2.6 nM), whereas no appreciable binding is observed in the AMF-activated form. *mP*, milli-Polarization units.

GDP·AlF_4^--bound) of Gα$_{i1}$^{WT}, Gα$_{i1}$^{E116L}, and Gα$_{i1}$^{Q147L} did not demonstrate any appreciable binding to the RGS14 GoLoco motif (Fig. 1); however, the aluminum tetrafluoride-activated Gα$_{i1}$^{E245L} was observed to bind the FITC-RGS14 GoLoco FP probe with a dissociation constant of 47 nM.

These affinity-enhancing mutations of Gα$_{i1}$ were computationally predicted based on the known structure of the WT Gα$_{i1}$/RGS14 GoLoco motif heterodimer (7, 27). To determine whether these mutations differentially affected binding to other known GoLoco motifs, we performed similar FP assays with GoLoco motifs from RGS12 and GPSM2 (the latter protein is also known as LGN or mammalian Pins). Both Gα$_{i1}$^{E116L}·GDP and Gα$_{i1}$^{E245L}·GDP had enhanced affinities toward the RGS12 and GPSM2 GoLoco motif FP probes, whereas the K_D values obtained for Gα$_{i1}$^{Q147L}·GDP were statistically indistinguishable from those for Gα$_{i1}$^{WT}·GDP for both probes (Fig. 2).

To determine the dissociation rates (k_{off}) of the WT and mutant Gα$_{i1}$ subunits from their respective complexes with the RGS12, RGS14, and GPSM2(GL2) GoLoco motifs, we used surface plasmon resonance biosensors. We generated surfaces of GST-RGS12 GoLoco, GST-RGS14 GoLoco, and GST-GPSM2(GL2) fusion proteins, each bound to separate anti-GST antibody-coated biosensor flow cells (30), and injected 200 μl of 50 nM Gα$_{i1}$^{WT}, Gα$_{i1}$^{E116L}, Gα$_{i1}$^{Q147L}, or Gα$_{i1}$^{E245L} (in their GDP-liganded forms). Dissociation rates were determined by fitting the resultant surface plasmon resonance sensorgrams (Fig. 3) with a single exponential dissociation function. RGS12 GoLoco motif-bound Gα$_{i1}$^{WT}, Gα$_{i1}$^{E116L}, Gα$_{i1}$^{Q147L}, and Gα$_{i1}$^{E245L} were observed to have k_{off} rates of 1.09, 0.85, 0.79, and 0.78 $(1000\ s)^{-1}$, respectively (Fig. 3*A*). Although the rates of dissociation from the RGS12 GoLoco motif were significantly decreased among all mutants *versus* WT Gα$_{i1}$, alterations in dissociation rates from the RGS14 GoLoco motif were more pronounced (Fig. 3*B*). Gα$_{i1}$^{E116L}, Gα$_{i1}$^{Q147L}, and Gα$_{i1}$^{E245L} had, respectively, 2-, 3-, and 4-fold decreases in their rates of dissociation compared with Gα$_{i1}$^{WT}. Gα$_{i1}$^{E116L} and Gαi1^{Q147L} also had significant, albeit modest, decreases in their rates of dissociation from GPSM2(GL2), 13.8 and 11.3 $(1000\ s)^{-1}$, respectively, compared with 14.8 $(1000\ s)^{-1}$ for Gα$_{i1}$^{WT}. By contrast, the rate of dissociation for Gα$_{i1}$^{E245L} was actually increased slightly to 16.6 $(1000\ s)^{-1}$.

Assessment of Nucleotide Binding and Hydrolysis Properties of the Affinity-enhanced Gα$_{i1}$ Mutants—Using our 2.2-Å crystal structure of the WT Gα$_{i1}$/RGS14 GoLoco motif interface (Protein Data Bank code 2OM2 (7)), we employed the Rosetta program to predict mutations with the goal of increasing GoLoco motif binding affinity while maintaining other Gα functionality. To determine whether the Gα$_{i1}$ mutants retain their ability to bind GTP, we performed radionucleotide-binding assays with [^{35}S]GTPγS. Whereas all three Gα$_{i1}$ mutants were capable of binding GTPγS, Gα$_{i1}$^{E245L} had a noticeably slower rate of binding (k_{obs}), 0.04 min^{-1} compared with

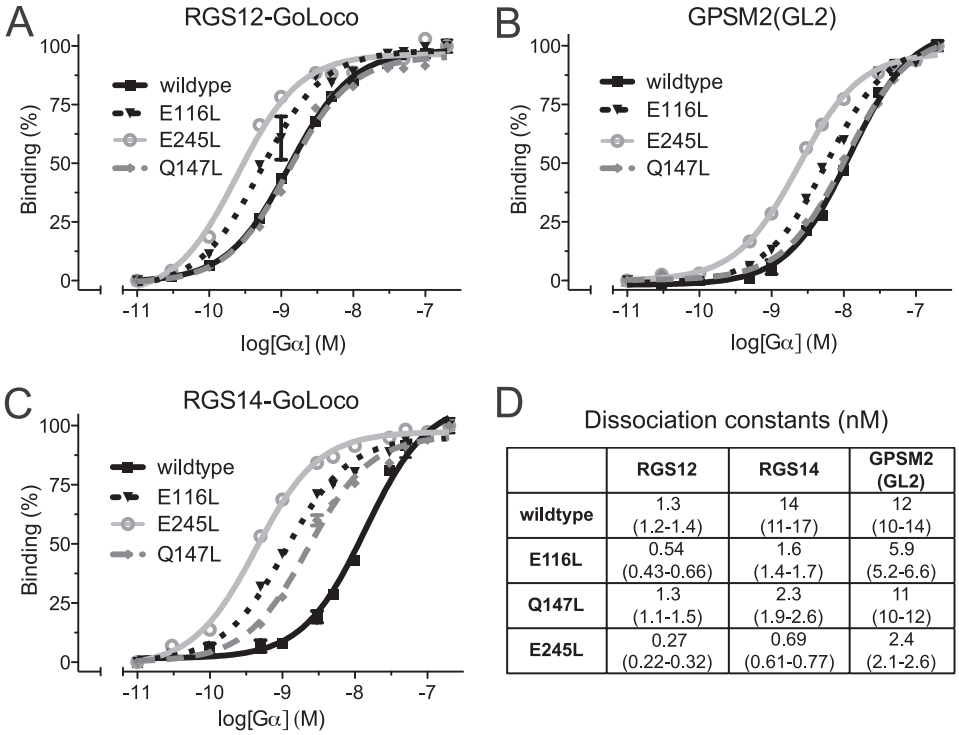

	RGS12	RGS14	GPSM2 (GL2)
wildtype	1.3 (1.2-1.4)	14 (11-17)	12 (10-14)
E116L	0.54 (0.43-0.66)	1.6 (1.4-1.7)	5.9 (5.2-6.6)
Q147L	1.3 (1.1-1.5)	2.3 (1.9-2.6)	11 (10-12)
E245L	0.27 (0.22-0.32)	0.69 (0.61-0.77)	2.4 (2.1-2.6)

FIGURE 2. **$G\alpha_{i1}$ point mutants exhibit enhanced affinity for multiple GoLoco motifs as measured by FP.** *A–C*, log linear binding isotherms were generated from FP measurements performed in triplicate and obtained by increasing the concentration of $G\alpha_{i1}$ to 200 nM while the FITC-GoLoco probe concentration was held constant at 350 pM. *D*, apparent dissociation constants (K_D) were calculated using nonlinear regression in GraphPad Prism. Values in *parentheses* represent 95% confidence intervals.

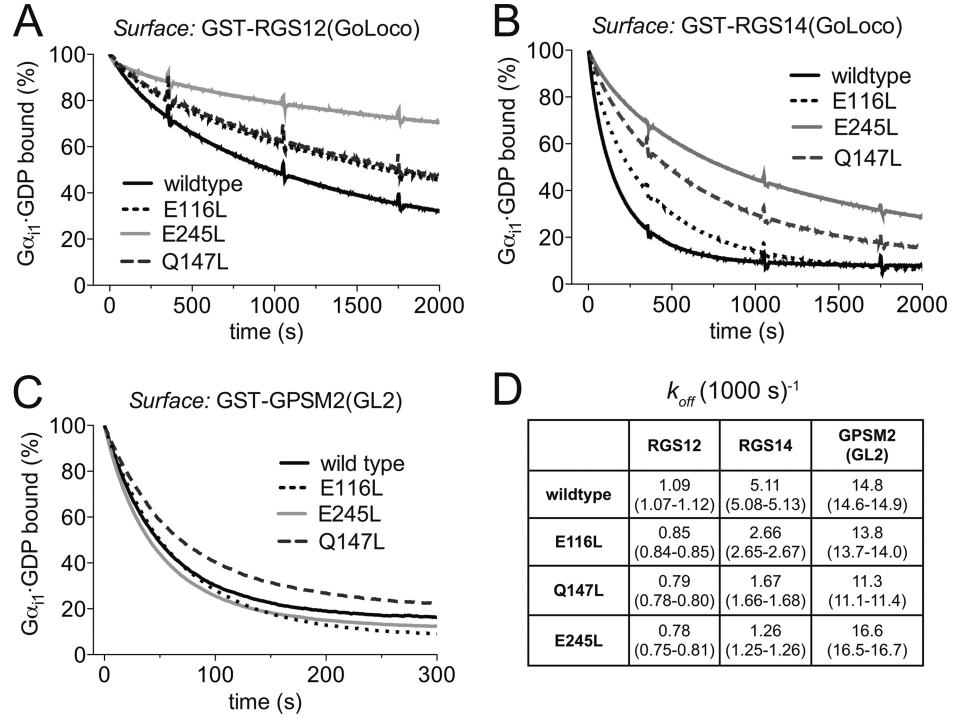

	RGS12	RGS14	GPSM2 (GL2)
wildtype	1.09 (1.07-1.12)	5.11 (5.08-5.13)	14.8 (14.6-14.9)
E116L	0.85 (0.84-0.85)	2.66 (2.65-2.67)	13.8 (13.7-14.0)
Q147L	0.79 (0.78-0.80)	1.67 (1.66-1.68)	11.3 (11.1-11.4)
E245L	0.78 (0.75-0.81)	1.26 (1.25-1.26)	16.6 (16.5-16.7)

FIGURE 3. **$G\alpha_{i1}$ point mutants exhibit decreased rates of dissociation from GoLoco motif complexes.** Surface plasmon resonance sensorgrams were generated by injecting 200 μl of 50 nM WT or mutant $G\alpha_{i1}$ over immobilized GST-RGS12 GoLoco motif (*A*), GST-RGS14 GoLoco motif (*B*), GST-GPSM2(GL2) (second GoLoco motif of LGN) (*C*), or GST alone at a flow rate of 40 μl/min with a dissociation phase of 2000 s. Dissociation curves are the plotted average of three independent experiments that have been normalized to percent of maximal binding. *D*, dissociation rates (k_{off}, expressed as per 1000 s) were derived from fitting to a single exponential function using GraphPad Prism. 95% confidence intervals are shown in *parentheses*.

0.07, 0.06, and 0.07 min^{-1} for $G\alpha_{i1}{}^{WT}$, $G\alpha_{i1}{}^{E116L}$, and $G\alpha_{i1}{}^{Q147L}$, respectively (Fig. 4*A*). To determine any effects on the intrinsic GTP hydrolysis rate, we also performed single-turnover [γ-^{32}P]GTP hydrolysis assays (Fig. 4*B*). $G\alpha_{i1}{}^{WT}$, $G\alpha_{i1}{}^{E116L}$, and $G\alpha_{i1}{}^{Q147L}$ were observed to have similar k_{cat} values of 0.48, 0.58, and 0.65 min^{-1}, respectively, whereas

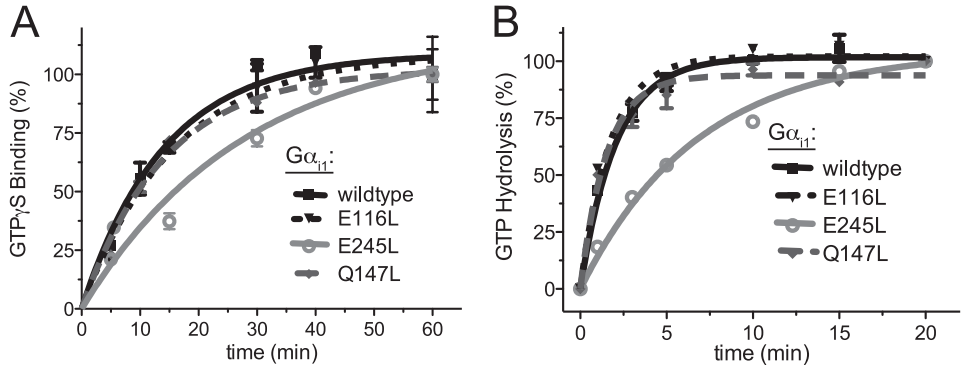

FIGURE 4. **Rates of guanine nucleotide binding and hydrolysis by affinity-enhanced Gα$_{i1}$ mutants.** *A*, nucleotide binding assays were initiated by the addition of [^{35}S]GTPγS to 100 nM WT or mutant Gα$_{i1}$ protein in either assay buffer or nonspecific buffer (the latter with excess unlabeled nucleotide). At the indicated time points, 100 μl of the protein mixture was vacuum-filtered through nitrocellulose, washed four times, and counted by scintillation. Assays were conducted in duplicate. The *error bars* represent S.E. Rates of binding (k_{obs}) were determined using nonlinear regression to be 0.07 min^{-1} (95% CI, 0.04–0.10), 0.04 min^{-1} (95% CI, 0.02–0.05), 0.06 min^{-1} (95% CI, 0.04–0.09), and 0.07 min^{-1} (95% CI, 0.06–0.08) for Gα$_{i1}$^{WT}, Gα$_{i1}$^{E245L}, Gα$_{i1}$^{E116L}, and Gα$_{i1}$^{Q147L}, respectively. *B*, intrinsic GTPase activities of WT and mutant Gα$_{i1}$ subunits were determined using [γ-^{32}P]GTP single-turnover assays. 100 nM Gα$_{i1}$ protein was loaded with [γ-^{32}P]GTP at 20 °C for 10 min before assays were initiated by the addition of Mg^{2+} (10 mM) and GTPγS (400 μM). At the indicated time points, 100 μl of the protein mixture was quenched with activated charcoal, and released [^{32}P]P$_i$ was counted by scintillation. Assays were conducted in duplicate. The *error bars* represent S.E. GTPase rates (k_{cat}) were determined using nonlinear regression to be 0.48 min^{-1} (95% CI, 0.40–0.56), 0.15 min^{-1} (95% CI, 0.12–0.17), 0.58 min^{-1} (95% CI, 0.46–0.70), and 0.65 min^{-1} (95% CI, 0.50–0.81) for Gα$_{i1}$^{WT}, Gα$_{i1}$^{E245L}, Gα$_{i1}$^{E116L}, and Gα$_{i1}$^{Q147L}, respectively.

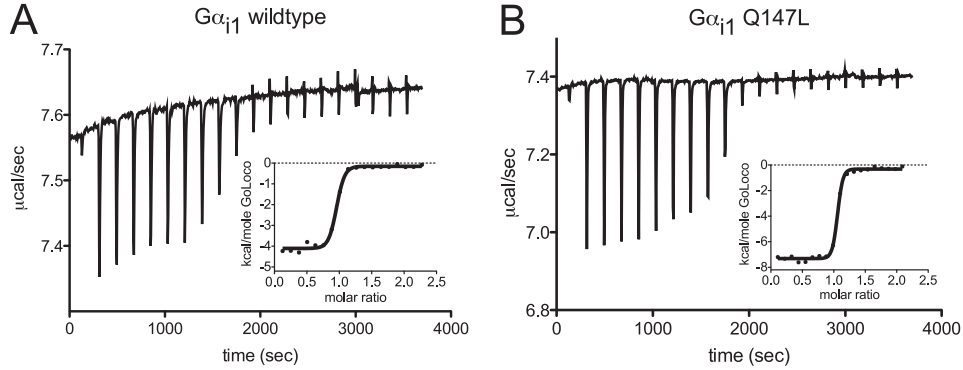

C

	Gα$_{i1}$^{wt}	Gα$_{i1}$^{Q147L}
ΔG (kcal/mol)	-10.7	-11.8
ΔH (kcal/mol)	-4.14 ± 0.44	-7.13 ± 0.24
ΔS (cal/mol/°C)	22.0	15.6

FIGURE 5. **Thermodynamic contributions to RGS14 GoLoco motif binding by WT and Gα$_{i1}$^{Q147L} subunits as determined by ITC.** 30 μM solutions of each indicated Gα$_{i1}$ subunit were separately titrated with repeated additions of 350 μM RGS14 GoLoco motif peptide. Calorimetric traces of heat released and enthalpic binding curves (*insets*) fitted with a one-site binding model are shown for Gα$_{i1}$^{WT} (*A*) and Gα$_{i1}$^{Q147L} (*B*). The stoichiometry of binding was ~1:1 in all experiments (three independent titrations were performed for each protein). *C*, average values and 95% confidence intervals for enthalpy of binding (Δ*H*) are given for the triplicate titration experiments ($p = 0.006$). Gibbs free energy (Δ*G*) is calculated from FP binding affinity measurements, and entropy of binding is derived by $\Delta S = (\Delta H - \Delta G)/T$.

Gα$_{i1}$^{E245L} had a reduced rate of GTP hydrolysis of 0.15 min^{-1} (95% confidence interval (CI), 0.12–0.17). Despite the rate changes observed with Gα$_{i1}$^{E245L}, all four Gα$_{i1}$ subunits demonstrated identical rates of activation by aluminum tetrafluoride, as measured by increased Trp-211 intrinsic fluorescence (supplemental Fig. S3). However, the reduced rates of GTP binding and hydrolysis exhibited by Gα$_{i1}$^{E245L} led us to exclude this particular mutant from further pursuit.

Assessment of Thermodynamic Binding Parameters of the Affinity-enhanced Gα$_{i1}$^{Q147L} Mutant—Rosetta makes predictions of changes in Gibbs free energy (Δ*G*) upon mutation of single residues, but because there is no explicit entropy term provided as output from the program, one cannot accurately predict whether affinity enhancement arises from favorable enthalpic (Δ*H*) or entropic (Δ*S*) thermodynamic changes (40). We therefore interrogated by isothermal titration calorimetry which thermodynamic parameter(s) were responsible for the higher affinity of GoLoco motif binding by Gα$_{i1}$^{Q147L} compared with Gα$_{i1}$^{WT} (Fig. 5). Enthalpy of binding was favorably exothermic for Gα$_{i1}$^{Q147L} at −7.13 kcal/mol compared with Gα$_{i1}$^{WT} at −4.14 kcal/mol, whereas entropy decreased unfavorably: 15.6 cal/mol/°C for Gα$_{i1}$^{Q147L} *versus* 22.0 cal/mol/°C for Gα$_{i1}$^{WT} (Fig. 5*C*).

Structural Determinants of the Gα$_{i1}$^{Q147L} Mutant Bound to the RGS14 GoLoco Motif—To elucidate the structural determinants of GoLoco affinity enhancement for Gα$_{i1}$^{Q147L}, we obtained x-ray diffraction data to 2.38-Å resolution from a single crystal of the Gα$_{i1}$^{Q147L}·GDP/RGS14 GoLoco motif peptide complex. A structural model was obtained by molecular replacement using the model of the WT Gα$_{i1}$·GDP/RGS14 complex

(Protein Data Bank code 2OM2) as a search model and subsequently refined (supplemental Table S1). The overall conformations of the $G\alpha_{i1}^{Q147L}$ subunit and bound GoLoco motif peptide were essentially identical (root mean square deviation of 0.38 Å, 2545 atoms used in comparison) (supplemental Fig. S1) to those observed in the WT crystal structure (7). The N-terminal helix of the RGS14 GoLoco motif contacts the Ras-like domain of $G\alpha_{i1}^{Q147L}$ in a manner similar to the WT structure (Protein Data Bank code 2OM2 (7)), whereas the N-terminal helix of a WT structure reported earlier (code 1KJY (13)) is shifted by one half-turn. The conserved (E/D)QR GoLoco triad (Asp-514, Gln-515, Arg-516) loops across the nucleotide-binding pocket, positioning the Arg-516 side chain to contact the α- and β-phosphate groups of GDP, and thus inhibits nucleotide dissociation (13). However, very weak electron density was observed for the preceding three GoLoco motif residues Gly-511, Ala-512, and His-513 that surround a well defined leucine side chain on $G\alpha_{i1}$ at position 147 (*i.e.* site of the Q147L substitution) (Fig. 6). Thus, the placement of a hydrophobic leucine on the surface of $G\alpha_{i1}$ appears to lead to disorder in the surrounding GoLoco motif peptide region. These findings suggest an increased conformational flexibility of the RGS14 GoLoco motif peptide in the region of amino acids 511–513 upon binding to $G\alpha_{i1}^{Q147L}$ compared with WT $G\alpha_{i1}$.

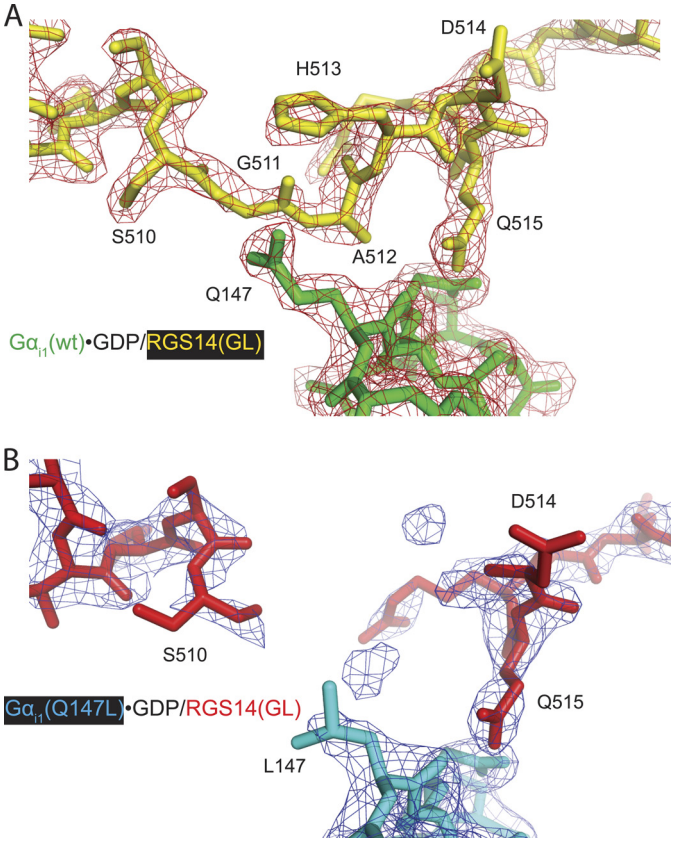

FIGURE 6. **Differences in electron density observed within the GoLoco motif between WT and Q147L mutant $G\alpha_{i1}$·GDP/RGS14 GoLoco motif complexes.** A crystal structure (using diffraction data to 2.38-Å resolution) of the $G\alpha_{i1}^{Q147L}$·GDP/RGS14 GoLoco motif complex (Protein Data Bank code 3ONW) was obtained. Overall, the $G\alpha_{i1}^{Q147L}$ protein binds the RGS14 GoLoco motif protein similarly (root mean square deviation of 0.38 Å) to $G\alpha_{i1}^{WT}$ (code 2OM2 (7)). However, electron density for the GoLoco motif peptide residues Gly-511, Ala-512, and His-513 is much weaker in the $G\alpha_{i1}^{Q147L}$ structure (*B*) than in the WT structure (code 2OM2) (*A*), indicating disorder in the peptide surrounding the mutated $G\alpha_{i1}$ residue Leu-147. Both $2F_o - F_c$ electron density maps shown are contoured at $\sigma = 1.5$.

Modeling of the Q147L Substitution by Monte Carlo Simulations—The $G\alpha_{i1}^{Q147L}$/GoLoco crystal structure suggest that residues 511–513 may be more dynamic in the mutant than in WT $G\alpha_{i1}$, and therefore, an increase in conformational entropy may contribute to the enhanced affinity of $G\alpha_{i1}^{Q147L}$ for GoLoco motifs. However, the ITC results show that the net change in the entropy component upon binding (Fig. 5) is more favorable for WT $G\alpha_{i1}$ than for $G\alpha_{i1}^{Q147L}$. In general, it is very difficult to predict relative changes in binding entropies and enthalpies because enthalpy/entropy compensation is a dominant feature of solvated systems (41). Changes in water networks in either the bound or unbound state could change the number of hydrogen bonds within the system and also change the rotational freedom of each water. Given our observation of disorder within the RGS14 GoLoco motif, we used Rosetta loop modeling simulations to examine the structural preferences of GoLoco motif residues 510–513 when bound to either $G\alpha_{i1}^{WT}$ or $G\alpha_{i1}^{Q147L}$. For each case, 100 independent structure prediction simulations were performed. With WT $G\alpha_{i1}$, all 100 simulations predicted a loop conformation similar to that observed in the crystal structure (Fig. 7*A*). However, with $G\alpha_{i1}^{Q147L}$, two alternative conformations were observed for residues 510–513 (Fig. 7*B*). In 40% of

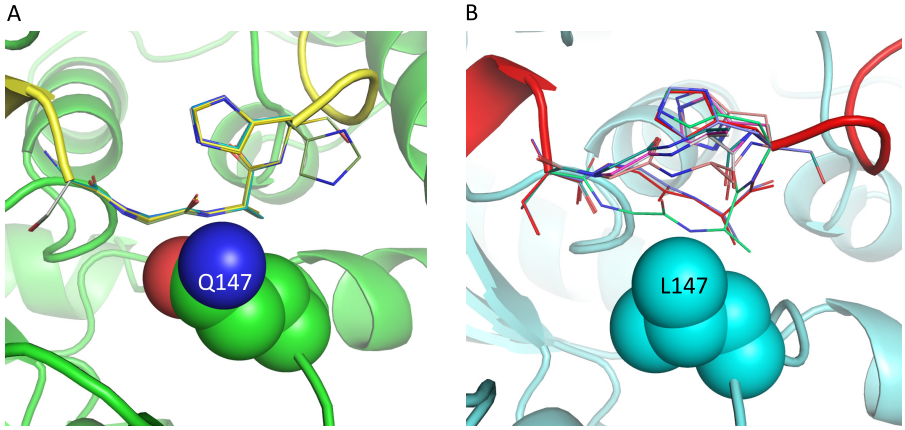

FIGURE 7. **Rosetta loop modeling predictions for the RGS14 GoLoco motif bound to $G\alpha_{i1}^{WT}$ and $G\alpha_{i1}^{Q147L}$.** Six representative models are shown from 100 independent structure prediction trajectories. GoLoco motif residues 510–513 are shown in stick mode. Gln-147 (*A*) and Leu-147 (*B*) are shown in space filling representation. Nitrogens are colored *blue*, and oxygens are colored *red*.

the models, residues 510–513 adopt a conformation similar to the WT structure; in the other 60%, residues 511 and 512 are displaced by >4 Å. The alternate conformation places the backbone groups adjacent to both methyl groups on the $G\alpha_{i1}$ residue Leu-147. The solvation energy term in Rosetta disfavors the alternate conformation for $G\alpha_{i1}{}^{WT}$ because both the nitrogen and oxygen atoms of Gln-147 are desolvated without the formation of a compensating hydrogen bond. These results are consistent with the poor electron density observed for residues 511–513 in the GoLoco/$G\alpha_{i1}{}^{Q147L}$ crystal structure.

Conclusions—Our findings confirm the ability of Rosetta to predict point mutations that enhance protein/protein binding affinities, a technique that should be readily applicable to other systems with high-resolution structural information available (7). Furthermore, our findings have provided insight into the kinetic, thermodynamic, and structural mechanisms underlying the favorable accommodation of affinity-enhancing mutations. Two of the three $G\alpha_{i1}$ mutants studied ($G\alpha_{i1}{}^{Q147L}$ and $G\alpha_{i1}{}^{E116L}$) exhibit enhanced binding to GoLoco motifs without disrupting guanine nucleotide binding or hydrolysis functions (an important consideration for their utility in examining selective $G\alpha$ activities in an integrated cellular context). The selective loss of GoLoco motif binding of the $G\alpha_{i1}{}^{N149I}$ point mutant was instrumental in establishing direct involvement of a $G\alpha_i$/GoLoco motif complex in microtubule dynamics underlying spindle orientation and chromosomal segregation during cell division (25). Other groups have since employed the $G\alpha_{i1}{}^{N149I}$ mutant to demonstrate that cell polarization-mediated spatial restriction of spindle orientation determinants is critical for epithelial morphogenesis (26) and that the multiple-GoLoco motif protein AGS4 may couple $G\alpha$ subunits to receptor-proximal events affected by agonist application (42). The verified gain-of-function mutants $G\alpha_{i1}{}^{Q147L}$ and $G\alpha_{i1}{}^{E116L}$ described in this work should complement the loss-of-function $G\alpha_{i1}{}^{N149I}$ mutant and find equal utility in investigating the role of $G\alpha$/GoLoco motif interactions in asymmetric cell division, epithelial progenitor differentiation, and G-protein-coupled receptor signaling regulation.

REFERENCES

1. Wu, Y. I., Frey, D., Lungu, O. I., Jaehrig, A., Schlichting, I., Kuhlman, B., and Hahn, K. M. (2009) *Nature* **461,** 104–108
2. Hahn, K. M., and Kuhlman, B. (2010) *Nat. Methods* **7,** 595–597
3. Woodnutt, G., Violand, B., and North, M. (2008) *Curr. Opin. Drug Discov. Dev.* **11,** 754–761
4. Leader, B., Baca, Q. J., and Golan, D. E. (2008) *Nat. Rev. Drug Discov.* **7,** 21–39
5. Rao, B. M., Lauffenburger, D. A., and Wittrup, K. D. (2005) *Nat. Biotechnol.* **23,** 191–194
6. Selzer, T., Albeck, S., and Schreiber, G. (2000) *Nat. Struct. Biol.* **7,** 537–541
7. Sammond, D. W., Eletr, Z. M., Purbeck, C., Kimple, R. J., Siderovski, D. P., and Kuhlman, B. (2007) *J. Mol. Biol.* **371,** 1392–1404
8. Kiel, C., Selzer, T., Shaul, Y., Schreiber, G., and Herrmann, C. (2004) *Proc. Natl. Acad. Sci. U.S.A.* **101,** 9223–9228
9. Reynolds, K. A., Hanes, M. S., Thomson, J. M., Antczak, A. J., Berger, J. M., Bonomo, R. A., Kirsch, J. F., and Handel, T. M. (2008) *J. Mol. Biol.* **382,** 1265–1275
10. Karanicolas, J., and Kuhlman, B. (2009) *Curr. Opin. Struct. Biol.* **19,** 458–463
11. Zahnd, C., Amstutz, P., and Plückthun, A. (2007) *Nat. Methods* **4,** 269–279
12. Sidhu, S. S., and Koide, S. (2007) *Curr. Opin. Struct. Biol* **17,** 481–487
13. Kimple, R. J., Kimple, M. E., Betts, L., Sondek, J., and Siderovski, D. P. (2002) *Nature* **416,** 878–881
14. Johnston, C. A., and Siderovski, D. P. (2007) *Mol. Pharmacol.* **72,** 219–230
15. Oldham, W. M., and Hamm, H. E. (2008) *Nat. Rev. Mol. Cell Biol.* **9,** 60–71
16. Willard, F. S., Kimple, R. J., and Siderovski, D. P. (2004) *Annu. Rev. Biochem.* **73,** 925–951
17. Sato, M., Blumer, J. B., Simon, V., and Lanier, S. M. (2006) *Annu. Rev. Pharmacol. Toxicol.* **46,** 151–187
18. Wiser, O., Qian, X., Ehlers, M., Ja, W. W., Roberts, R. W., Reuveny, E., Jan, Y. N., and Jan, L. Y. (2006) *Neuron* **50,** 561–573
19. Iscru, E., Serinagaoglu, Y., Schilling, K., Tian, J., Bowers-Kidder, S. L., Zhang, R., Morgan, J. I., DeVries, A. C., Nelson, R. J., Zhu, M. X., and Oberdick, J. (2009) *Mol. Cell. Neurosci.* **40,** 62–75
20. Blumer, J. B., Lord, K., Saunders, T. L., Pacchioni, A., Black, C., Lazartigues, E., Varner, K. J., Gettys, T. W., and Lanier, S. M. (2008) *Endocrinology* **149,** 3842–3849
21. Colombo, K., Grill, S. W., Kimple, R. J., Willard, F. S., Siderovski, D. P., and Gönczy, P. (2003) *Science* **300,** 1957–1961
22. Yu, F., Morin, X., Kaushik, R., Bahri, S., Yang, X., and Chia, W. (2003) *J. Cell Sci.* **116,** 887–896
23. Schaefer, M., Shevchenko, A., Shevchenko, A., and Knoblich, J. A. (2000) *Curr. Biol.* **10,** 353–362
24. Du, Q., Stukenberg, P. T., and Macara, I. G. (2001) *Nat. Cell Biol.* **3,** 1069–1075
25. Willard, F. S., Zheng, Z., Guo, J., Digby, G. J., Kimple, A. J., Conley, J. M., Johnston, C. A., Bosch, D., Willard, M. D., Watts, V. J., Lambert, N. A., Ikeda, S. R., Du, Q., and Siderovski, D. P. (2008) *J. Biol. Chem.* **283,** 36698–36710
26. Zheng, Z., Zhu, H., Wan, Q., Liu, J., Xiao, Z., Siderovski, D. P., and Du, Q. (2010) *J. Cell Biol.* **189,** 275–288
27. Sammond, D. W., Eletr, Z. M., Purbeck, C., and Kuhlman, B. (2010) *Proteins* **78,** 1055–1065
28. Kimple, A. J., Yasgar, A., Hughes, M., Jadhav, A., Willard, F. S., Muller, R. E., Austin, C. P., Inglese, J., Ibeanu, G. C., Siderovski, D. P., and Simeonov, A. (2008) *Comb. Chem. High Throughput Screen.* **11,** 396–409
29. Kimple, R. J., De Vries, L., Tronchère, H., Behe, C. I., Morris, R. A., Gist Farquhar, M., and Siderovski, D. P. (2001) *J. Biol. Chem.* **276,** 29275–29281
30. Hutsell, S. Q., Kimple, R. J., Siderovski, D. P., Willard, F. S., and Kimple, A. J. (2010) *Methods Mol. Biol.* **627,** 75–90
31. McCudden, C. R., Willard, F. S., Kimple, R. J., Johnston, C. A., Hains, M. D., Jones, M. B., and Siderovski, D. P. (2005) *Biochim. Biophys. Acta* **1745,** 254–264
32. Afshar, K., Willard, F. S., Colombo, K., Johnston, C. A., McCudden, C. R., Siderovski, D. P., and Gönczy, P. (2004) *Cell* **119,** 219–230
33. Johnston, C. A., Lobanova, E. S., Shavkunov, A. S., Low, J., Ramer, J. K., Blaesius, R., Fredericks, Z., Willard, F. S., Kuhlman, B., Arshavsky, V. Y., and Siderovski, D. P. (2006) *Biochemistry* **45,** 11390–11400
34. Higashijima, T., Ferguson, K. M., Sternweis, P. C., Ross, E. M., Smigel, M. D., and Gilman, A. G. (1987) *J. Biol. Chem.* **262,** 752–756
35. Wall, M. A., Posner, B. A., and Sprang, S. R. (1998) *Structure* **6,** 1169–1183
36. Otwinowski, Z., and Minor, W. (1997) *Methods Enzymol.* **276,** 307–326
37. McCoy, A. J., Grosse-Kunstleve, R. W., Adams, P. D., Winn, M. D., Storoni, L. C., and Read, R. J. (2007) *J. Appl. Crystallogr.* **40,** 658–674
38. Collaborative Computational Project (1994) *Acta Crystallogr. D Biol. Crystallogr.* **50,** 760–763
39. Emsley, P., Lohkamp, B., Scott, W. G., and Cowtan, K. (2010) *Acta Crystallogr. D Biol. Crystallogr.* **66,** 486–501
40. Kortemme, T., and Baker, D. (2002) *Proc. Natl. Acad. Sci. U.S.A.* **99,** 14116–14121
41. Brady, G. P., and Sharp, K. A. (1997) *Curr. Opin. Struct. Biol.* **7,** 215–221
42. Oner, S. S., Maher, E. M., Breton, B., Bouvier, M., and Blumer, J. B. (2010) *J. Biol. Chem.* **285,** 20588–20594